Sensors & Actuators: B. Chemical 371 (2022) 132505

Contents lists available at ScienceDirect

Sensors and Actuators: B. Chemical

journal homepage: www.elsevier.com/locate/snb

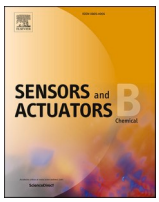

# A portable and smartphone-based plasmonic system for on-site measurement of airborne redox-active compounds by light-initiated redox reaction

Ranxue Yu [a,b,c], Guangyu Qiu [b,c,d,*], Yi-Bo Zhao [b,c], Denise Freudemann [e], Beatrice Fisher [f], Xinhou Wang [a,g,**], Jing Wang [b,c,***]

[a] Key Laboratory of Textile Science and Technology of Ministry of Education, College of Textiles, Donghua University, Shanghai 201620, China
[b] Institute of Environmental Engineering, ETH Zurich, Zurich 8093, Switzerland
[c] Advanced Analytical Technologies, Empa, Ueberlandstrasse 129, Dübendorf 8600, Switzerland
[d] Institute of Medical Robotics, Shanghai Jiao Tong University, Dongchuan Road, Shanghai 200240, China
[e] Eawag, Swiss Federal Institute of Aquatic Science and Technology, Dübendorf 8600, Switzerland
[f] Laboratory for Functional Polymers, Empa, Ueberlandstrasse 129, Dübendorf 8600, Switzerland
[g] College of Mechanical EnV, Shanghai 201620, China

ARTICLE INFO

*Keywords:*
Airborne redox-active compounds
Gold nanoparticles
Light-mediated photochemistry reaction
Smartphone
Real-world aerosols

ABSTRACT

The determination of airborne redox-active compounds (ARC) is essential for monitoring adverse environmental changes and understanding the potential impact on human health. With the exception of relying on the common total organic carbon (TOC) analyzer and dithiothreitol (DTT) assay, there is currently no easy-to-use method for quantitative assessment. Herein, a compatible and easy-to-use colorimetric sensing strategy was developed for on-site ARC quantification. This approach integrated a plasmonic sensing system, where the ARC-induced gold nanoparticles (AuNPs) reduction, localized surface plasmon resonance (LSPR), and the light-mediated photochemistry collaborated to achieve a limit of detection (LOD) at 0.05 μg•mm$^{-2}$ on the filters. Distinguished from the abovementioned methods, the ARC content can be directly determined by in-situ monitoring the colorimetric reaction on the sampling quartz filters (QF) without additional sample pre-treatment. Apart from utilizing the standard benchtop photodetector (e.g., UV–VIS spectrophotometer), the colorimetric images of AuNP@QF samples could also be imaged by a smartphone camera in a sealed box and analyzed through a smartphone-based application to read the RGB (Red, Green, Blue) values for ARC quantification. The good correlation between the results using the spectrophotometer and smartphone validate the applicability of the AuNP sensor. The smartphone-based method was then deployed to test real-world aerosols collected from Zurich, Bern and Rigi and the results of ARC exhibited a positive correlation with that of PM10. With the advantages of low-cost, easy-operation and no need for pre-treatment, this smartphone-based plasmonic system holds great potential for rapid and portable ARC detection and corresponding air quality assessment.

## 1. Introduction

The presence of airborne redox-active compounds (ARC) has been found to be associated with adverse effects on human health such as cardiopulmonary disease and lung cancer. [20,29] Mounting evidences strongly support the hypothesis that the toxic effects of ARC are derived from the generation of reactive oxygen species (ROS), resulting in the induction of oxidative stress. [32,38] Many chemical species in airborne particles are considered redox-active, mainly including quinones [28, 49], transitional metals (e.g., manganese (Mn) and copper (Cu)) [10], humic-like substances, [32] soot or black carbon, [2,36] and secondary organic aerosols (SOA). [12] Among these compounds, quinones and transitional metals are widely recognized as the main contributors. In fine particulate matter, the concentrations of soluble transition metals

* Corresponding author at: Institute of Medical Robotics, Shanghai Jiao Tong University, Dongchuan Road, Shanghai 200240, China.
** Correspondence to: Donghua University, 2999 North Renmin Road, Songjiang District, Shanghai 201620, China.
*** Correspondence to: Institute of Environmental Engineering, ETH Zurich, Zurich, Switzerland.
*E-mail addresses:* guangyuqiu@sjtu.edu.cn (G. Qiu), xhwang@dhu.edu.cn (X. Wang), jing.wang@ifu.baug.ethz.ch (J. Wang).

https://doi.org/10.1016/j.snb.2022.132505
Received 24 April 2022; Received in revised form 29 July 2022; Accepted 9 August 2022
Available online 10 August 2022

are generally higher than those of quinones and thus metals are significant contributors to oxidative potential [34].

Diverse analytical methods have been investigated to realize the qualitative and quantitative analyses of ARC. Previous studies have reported that the chemical composition of certain ambient particles can be quantitatively analyzed by gas chromatography with mass spectrometry (GC-MS), [14] proton nuclear magnetic resonance (NMR), [40] high-resolution time-of-flight aerosol mass spectrometry (HR-TOF-AMS), [13] inductively coupled plasma-mass spectrometry (ICP-MS) [16] and so on. These previous reports revealed that the mass loading of quinones in ambient particles was generally below 1 ng/$m^3$ [38], [14] while Fe is the most abundant ARC compound with the concentration range of 6.4–196 ng/$m^3$, typically followed by Cu. [11] Carbon quantifications based on converting the organic compounds into $CO_2$ are also unequivocal determination methods for organic ARC compounds. These techniques can offer good limits of detection and wide linear ranges, but are very expensive and require considerable expertise. Additionally, carbon quantification approaches, such as the TOC analyzer can only measure organic ARC species while ignoring the presence of abundant redox-active transition metals. Furthermore, the TOC analyzer requires additional sample pre-treatment and estimated concentration range. It remains challenging to quantify the total redox-active compounds through the aforementioned techniques due to the complexity and variability in the chemical compositions of ARC. A widely used method based on the oxidative ability of ARC to quantify the redox activity of ARC and its potential to generate ROS has been developed. [10] This assay measures the consumption rate of DTT and subsequently quantifies the ARC concentration based on the linear correlations between DTT consumption and ARC concentrations. However, this DTT-based approach still requires airborne particle extraction before the analysis. Therefore, there is an urgent demand for a rapid, facile, flexible and cost-effective method for in-situ determination of ARC on filters without the need for extraction particles.

Recent progress has seen a sharp uptick in the manufacturing of metal-engineered nanomaterials, especially silver and gold nanoparticles (Ag and AuNPs) due to their potential applications in diverse fields, such as surface-enhanced Raman scattering, photocatalysis, plasmonic sensors, and imaging, *etc*,. [44,46,48] Specifically, diverse sensors based on the alteration of localized surface plasmon resonances (LSPR) properties have been developed for the detection of heavy metals, DNA, and protein biomarkers. [3,47] Of particular interest is the flexible and easy-to-use colorimetric sensor based on measuring the absorbance and color change with the aid of photodetectors. Moreover, colorimetric methods developed with smartphones for digital images have been applied to determine ozone and nitrogen dioxide, [24,8,9] glucose and cholesterol, [26] pH values. [31] Instead of sophisticated instruments such as spectrophotometer, the smartphone-based reader provides a facile and cost-effective platform for accurate quantification.

Several previous studies have suggested that diverse organic matters [33,45,51] containing phenolic compounds in nature could be used to synthesize AuNPs. Some of them have indicated that hydroquinone/quinones [1,53] are effective reductants for reducing different metal ions such as Au and Cu. The phenolic, aldehyde and alcoholic groups in these organic matters are considered to have an affinity to metal ions and be capable of complexation and reduction of metal ions. [23,51] Earlier studies have also substantiated the ubiquitous presence of airborne *p*-benzoquinone (BQ), with an average concentration of 1.6 ng• $m^{-3}$ in the gas and particle phase. [21] These airborne BQ could act as electron donors for the reduction of AuNPs after light irradiation. [33, 39] Considering the simple structure and redox ability of BQ, we selected BQ as the standard ARC model in this work.

This work aimed to develop a simple, fast and cost-effective colorimetric method for the direct determination of ARC on the filters by the combination of the colorimetric response of AuNPs and the reduction capability of ARC. As a convenient and commonly used aerosol sampling filter, QF can be directly employed for airborne particles collection. Additionally, the filter-based substrates have a high surface area and the capability to store reactants in the active form within the fiber network. In this work, we deposited airborne BQ particles on the QF and subsequently achieved in-situ reduction of gold ions through light irradiation. The colorimetric response of the ARC-reduced AuNPs could be directly quantified by measuring the reflectance of the filter through a standard benchtop UV–VIS spectrophotometer. Moreover, the entire analytical system could be integrated into a portable device by exploiting the smartphone-based camera and digital image processing software. The RGB values of the smartphone images were extracted for quantifying the concentration of ARC. The results from the proposed smartphone assay showed strong correlations with the standard UV–VIS spectroscopic results. The proposed method was then deployed to test real-world airborne samples collected from three different sites in Zurich, Bern and Rigi. This low-cost and flexible analytical approach offers outstanding advantages over the conventional ARC analysis techniques, including the elimination of sample extraction, improved detection efficiency, simple operation, fast on-site ARC quantification, and exemption of complex and expensive analytical instrumentation.

## 2. Experiment section

### 2.1. Chemicals

Gold (III) chloride solution (99.99 %) and *p*-Benzoquinone (BQ) were purchased from Sigma (St. Louis, Mo). All chemicals were in analytical grade and used without further purification. A 100 mg/L BQ solution was prepared by dissolving 100 mg BQ in 1 L of deionized water.

### 2.2. Standard samples collection and characterization

BQ particles were generated using a home-made atomizer at a pressure of 3 bar with a flow rate of 3.8 L/min and dried by a diffusion dryer. Then the particles were collected on the QF in a filter holder. The collection setup was shown in Fig. S1. In this study, the BQ particles were collected on filters for 5, 10, 15, 30, 45, 60, 90, 120, 150 and 180 min. The TOC analyzer with a detection limit of 0.5 mg/L was used to measure the concentration of dissolved organic carbon on the QF. The particle size distribution (i.e., electrical mobility diameters) of the generated BQ particles was measured by a scanning mobility particle sizer (SMPS) (Fig. S2) consisting of a Differential Mobility Analyzer (DMA, model 3080, TSI, USA) and a Condensation Particle Counter (CPC, model 3775, TSI, USA). The DMA was employed to select particles with the target diameter. The CPC was used to count the particles in the monodisperse sample from the DMA.

To measure the filtration efficiency of QF, A DMA (model 3082, TSI, USA) and two CPCs were used. The NaCl particles with mobility diameters of 30, 50, 100, 200, 300, 400, 500, 600 nm were selected through the DMA. The particle numbers before ($C_{up}$) and after ($C_{down}$) the filters were determined by CPCs. The collection efficiency ($\eta$)was calculated based on the following Eq. (1):

$$\eta = \frac{C_{up-}C_{down}}{C_{up}} \times 100\% \quad (1)$$

The pore size and distribution of QF were measured by a Porometer (Porolux 1000).

### 2.3. Procedures for ARC quantification based on reflectance by UV–VIS spectrophotometer and digital image colorimetry by a smartphone

The $HAuCl_4$ precursor with a concentration of 12.7 mM was sprayed on the QF with ARC using a sprayer (Fig. S3). The total mass of the $HAuCl_4$ precursor on the filter was set as about 0.12 g. These mixtures were irradiated with visible light of a xenon lamp (Model Nr. FL-302 E) at 0.204 W / 5 cm to accelerate the chemical reduction of AuNPs on the filters. The basic analytical concept was to quantify the LSPR

colorimetric effect of the BQ-reduced AuNPs and measure the reflectance of QF using the UV–VIS-NIR spectrophotometer (SHIMADZU, UV-3600). The alternative quantitative measurement approach was based on the color images of AuNPs using a smartphone device. The constructed visual detection device consisted of white lamp, a sealed imaging box and a smartphone. The device had an overall dimension (LWH) of ~160 mm × 87 mm × 50 mm with a dedicated imaging window (LW) of ~35 mm × 35 mm on the top of the box. The smartphone was placed on the top of the box, with the camera lens aligned with the imaging window. Inside the box, lamp were placed to illuminate the filter sample, and the sample was fixed at the bottom just below the imaging window. A high-resolution photograph using the back camera of an iPhone 13 in the automatic mode with the flash turned off was subsequently processed in the RGB color space with the Color Swatch app. The detail of a scheme of experiment setup for smartphone were shown in the supporting information S1. After data processing, the analytical signal was calculated from the G channel using Eq. (2). [7-9] Then a standard curve with respect to Log ($G_s/G_b$) versus the target content can be easily established.

$$EA_G = Log \quad (\frac{G_b}{G_s}) \tag{2}$$

Where $EA_G$ is the effective absorbance, $G_s$ is the mean value of the individual G channel from samples with ARC and $G_b$ is the mean value of the individual G channel from the blank samples without ARC.

The surface morphologies of the QF were characterized by field emission scanning electron microscopy (FE-SEM, Nova NanoSEM 230, FEI company, Hillsboro, OR, USA). The surface morphologies and element analysis of the QF after deposition of BQ particles and after the redox reaction under light irradiation were further analyzed by field emission scanning electron microscopy equipped with energy dispersive spectrum (EDS) accessory (FE-SEM, SU8010, Hitachi, Japan). The morphologies and diffraction pattern of AuNPs was analyzed by transmission electron microscopy (TEM) with accelerating voltage 150 KV (JEM 2100). The crystalline structures of the QF before and after the redox reaction were evaluated by X-ray diffraction (XRD, PANalytical X'Pert PRO diffractometer equipped with Cu Kα radiation).

### 2.4. Collection and ARC quantification of environmental aerosol-on-filter samples

Aerosol sampling was carried out at three sites of the Swiss National Air Pollution Monitoring Network (NABEL). The daily specimens were from Zurich (Kaserne, an urban background area), Bern (Bollwerk, an urban traffic area) and Rigi (Seebodenalp, a rural area). The measurements were performed from 1 July to 31 July and 1 December to 31 December 2020.

The sampling station in Zurich was located in a park-like courtyard in the center of the metropolitan area of Zurich (approx. 500 m west of the main train station), which was part of the building complex of the old barracks and had a dense population. The sampling station in Bern was aligned on both sides with a multi-story row of houses and near the traffic roadside which had approximately 20,000–30,000 vehicles passing by every day. The last station in Rigi was situated on the northern slope of Rigi Mountain with a high-altitude above 1000 m.a.s.l, as a rural environment setting surrounded by alternative pasture land and forest areas.

A high-volume sampler (DH-80, Digitel) was employed to collect particles less than 10 μm in aerodynamic diameter (PM10) on the pre-baked QF. The sampling flow rate was 500 L/min. Filters were collected every two days in Zurich and Bern, while samples in Rigi were collected every day. After sampling, all filters were stored in a freezer at −20 °C until analysis. With a puncher, portions of filters with diameters of 20 mm were extracted. In this work, daily particulate matter samples from July and December were used for analysis without any pretreatment. The ARC concentrations of the real-word samples were obtained by integrating the $EA_G$ value of a sample into the standard linear equation.

## 3. Results and Discussion

### 3.1. Light-induced ARC redox reaction for the formation of AuNPs mechanism

The light-induced ARC redox reaction process was depicted in Fig. 1. Given the standard redox potentials of reactants (0.699 V for BQ [15] while 1.002 V for $Au^{3+}$ in acid condition [35]), the reduction reaction can naturally occur at room temperature. Therefore, the formation of AuNPs was mainly governed by the presence of reducing agent, e.g., BQ on the filters, while the light irradiation further accelerated the BQ-assisted photochemical reduction of gold ions to AuNPs to be finished within 20 min. This photochemical reduction has also been verified in previous work. [39] Additionally, BQ also served as stabilizers [37] for the in-situ generated AuNPs on the filters. As shown in Fig. S4, COO-, C═O of carbonyl (1640 $cm^{-1}$) in BQ could act as reduction sites that were capable of reducing metal ions to metal atoms. [22] As one of the known ARC moieties, BQ compounds are ubiquitous in environmental samples at various concentrations. [27,54] Therefore, BQ was chosen as the standard ARC model in this work. The ARC concentrations in the aerosols determined the extent of the ARC-oxidant (i.e., gold ions) interactions, and subsequently the absorption intensity of AuNPs. Therefore, the ARC quantification can be achieved by measuring the optical response through UV–VIS spectroscopy or analyzing digital imaging through a smartphone.

### 3.2. The filtration performance of QF

In this work, the filters we adopted were not only used as a reservoir to store $HAuCl_4$ reagents for in-situ AuNPs redox reaction but also served as the sampling filters for collecting aerosols. Previous studies have indicated that the particle mobility diameter and trapped mass of particles within the filter are the dominant parameters to evaluate the filter performance. [50] There are mainly five mechanisms including diffusion, interception, inertial impaction, gravity settling and electrostatic effects for filtration. When the diameters of particles are less than 0.1 μm, diffusion is the governing mechanism. Herein, an aqueous solution of 100 mg/L BQ was used to generate soluble BQ particles with an arithmetic mean diameter of 64.1 ± 0.2 nm (Fig. 2b). For the range of particle size in this study, BQ particles were mainly captured by filters via the diffusion mechanism. As the trapped mass of particles became high, interception would take effect in addition to the diffusion effect. Additionally, the filter structure plays an important role in filtration. The mean pore size of the filter we adopted in this study was 2.96 μm, which was suitable for BQ particles retention via diffusion and

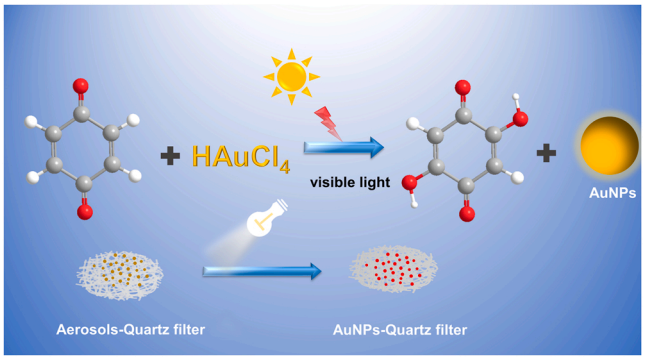


**Fig. 1.** Schematic diagram of light-induced AuNP sensor for on-site determination of airborne redox-active compounds on the filters.

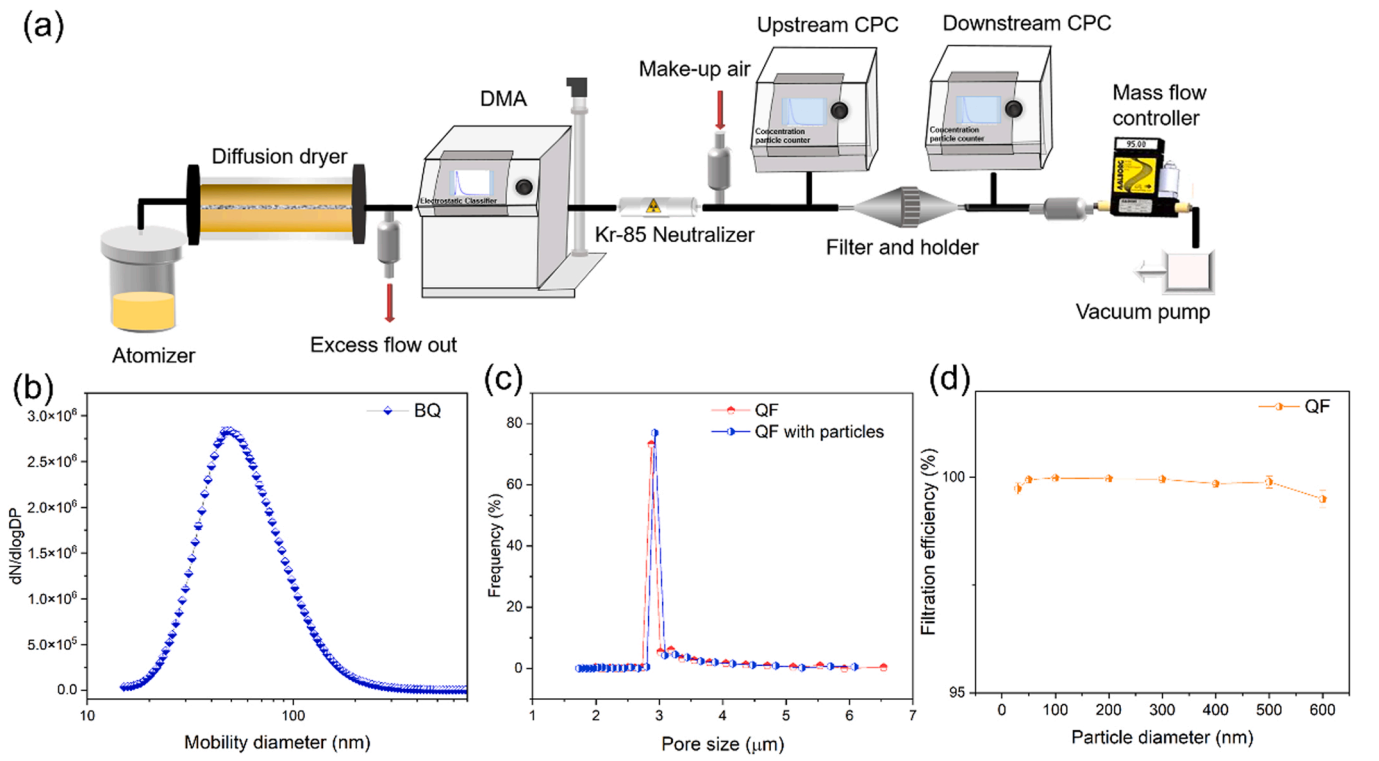


**Fig. 2.** (a) Setup for the NaCl particles collection efficiency evaluation; (b) Particle number size distribution of the BQ particles; (c) Pore size distribution of QF before and after deposition of particles for 180 min; (d) Filtration efficiency of the clean QF for NaCl particles in the size range of 30–600 nm.

interception. Additionally, the pore size distribution (PSD) affected particle motion. [4] A narrow PSD in this work made particles move slowly, further increasing the filtration efficiency. Fig. 2c showed similar mean pore sizes and distribution before and after the particles deposition, indicating that the BQ deposition within the adopted sampling time (e.g., 180 min) had a negligible effect on the pore size and distribution. By increasing the deposition time from 5 to 180 min, the total organic mass of BQ particles loaded on per square milimeter of filters increased from 0.026 to 0.49 μg/mm$^2$ (Fig. S5). The color of the filter also varied from light yellow to dark brown (Fig. S6).

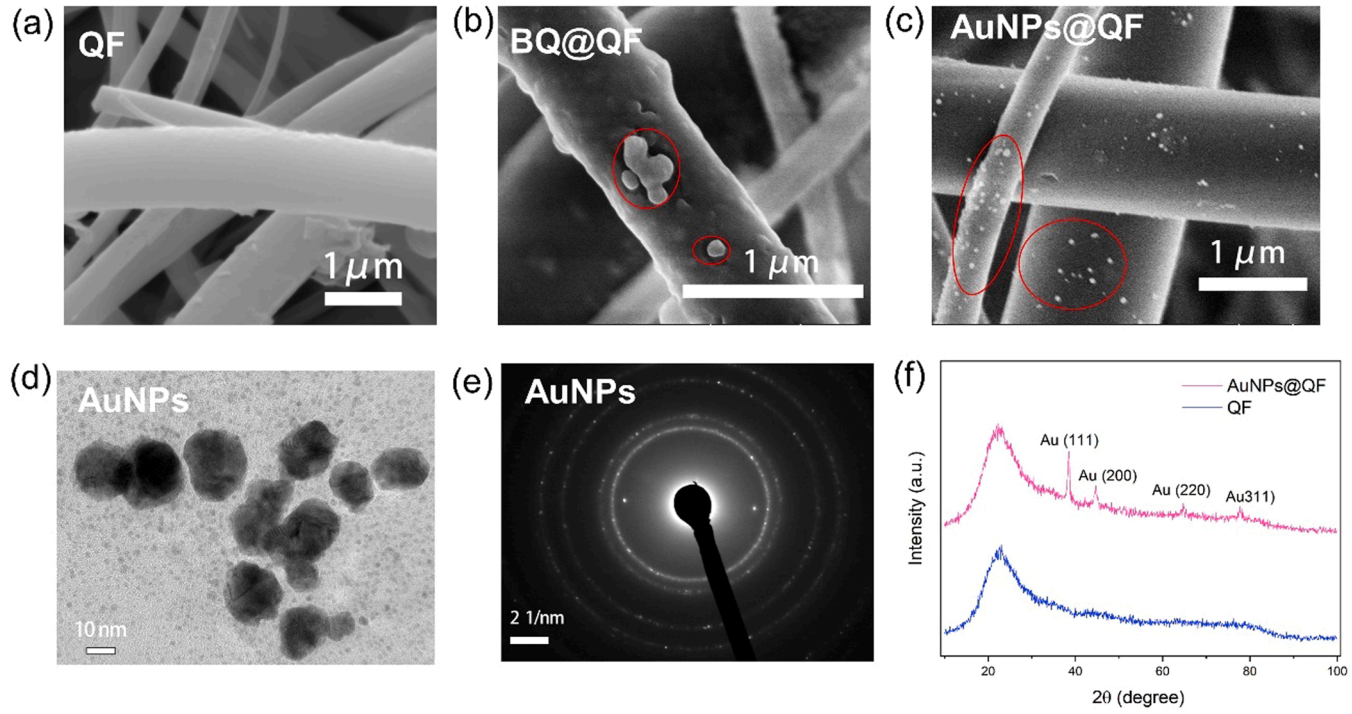


**Fig. 3.** SEM images of (a) pristine QF, (b) BQ@QF and (c) the AuNPs@QF; (d) TEM image and (e) corresponding SAED patterns of the AuNPs extracted from the QF in the condition of deposition time for 180 min; (f) XRD patterns of QF and AuNPs@QF.

The schematic setup for the filtration efficiency test was shown in Fig. 2a. Herein, NaCl particles were generated by an atomizer and dried through a diffusion dryer. Then, the targeted mobility diameters were selected with a DMA. A Kr-85 neutralizer after the DMA was employed to neutralize the monodisperse particles and minimize the filtration efficiency induced by electrostatic forces. [42] Fig. 2d showed the size-resolved filtration efficiencies for a clean QF. Overall, the size-resolved filtration efficiency was higher than 99 % for particles in the size range of 30–600 nm, demonstrating the good filtration performance of QF for collecting BQ particles.

### 3.3. Characterization of AuNPs on the QF and optical response for BQ particles

Fig. 3(a), (b) and (c) showed the structural morphologies of QF, BQ@QF and AuNPs@QF. The pristine QF has a typically porous structure of nonwoven matrix with fiber diameters of 0.16–1.5 μm. Upon deposition BQ particles for 180 min, we could observe BQ particles on the surface of QF fibers (Fig. 3b and S7). After irradiation with visible light, we found the formation of AuNPs on the fiber surface (Fig. 3c and S7). After the AuNP formation, the color of the QF substrate varied from brown to pink. Furthermore, we extracted the AuNPs on the QF into deionized water and investigated AuNPs using comprehensive characterizations including TEM and SAED. The TEM images and SAED patterns demonstrated the sphere-like AuNPs with a crystalline face-centered cubic (fcc) lattice structure (Figs. 3d and 3e). From inner to outer, the rings correspond to (111), (200), (220), and (311) reflections. As shown in Fig. 3f, the XRD spectrum of AuNPs@QF demonstrated the standard polycrystalline peaks of Au (111), (200), (220), and (311), which was consistent with the result of SAED patterns in Fig. 3e. The above-mentioned characterizations confirmed the successful BQ-mediated reduction of AuNPs by irradiation with visible light.

Subsequently, the concentration-dependent photochemical reduction of AuNPs was further investigated with different BQ concentrations. The standard BQ particles with organic mass ranging from 0.026 to 0.49 μg/mm$^2$ on the QF were analyzed in triplicate, and the reflectance spectra collected from different AuNPs@QFs were consequently depicted in Fig. 4a. The blank sample ($HAuCl_4$ and bare QF) was used as the reference for evaluating LOD. The detailed calculating method was provided in the supporting information S2. The reflectance intensities at 520 nm generally decreased with the increase of total organic mass concentrations of BQ particles loaded on per square millimeter of filters from 0.026 to 0.49 μg/mm$^2$. Furthermore, the linear relationship was studied and the sensor demonstrated a satisfactory correlation between the BQ mass and reflectance intensity. The reflectance responses of AuNPs data were integrated into a single calibration curve as shown in Fig. 4b. The fitting of the calibration graph generated a reference regression equation: $y = -71.81x + 62.30$; $R^2 = 0.992$. The data for calculating LOD were added in the supporting information Table S2. Due to actual UV–VIS signals at lower concentrations higher than that of the linear curve, we performed an additional linear fitting (Fig. 4b inset) to the range of 0.026–0.257 μg/mm$^2$. Thereby, we determined that the UV–VIS-based sensing approach had a LOD as low as 0.004 μg/mm$^2$ (Table S3). Meanwhile, the color of filters changed from light pink to violet along with the increase of target total organic mass concentrations of BQ particles loaded on per square millimeter of filters (Fig. 4c). The color variation provided the foundation for the development of a portable device for the visual sensing of ARC on the filters. Furthermore, this sensor system has a broad linear dynamic range from 0.026 μg/mm$^2$ to 0.49 μg/mm$^2$ and a comparable LOD (0.004 μg/mm$^2$, requiring at least about 0.314 μg aerosols mass in a filter area with a diameter of 10 mm), when compared with the TOC method (0.5 mg/L, requiring at least about 5 μg aerosols mass with a volume of 10 ml) for monitoring ARC.

### 3.4. Smartphone-based visual detection of BQ particles

To further investigate the on-site application potential, we then

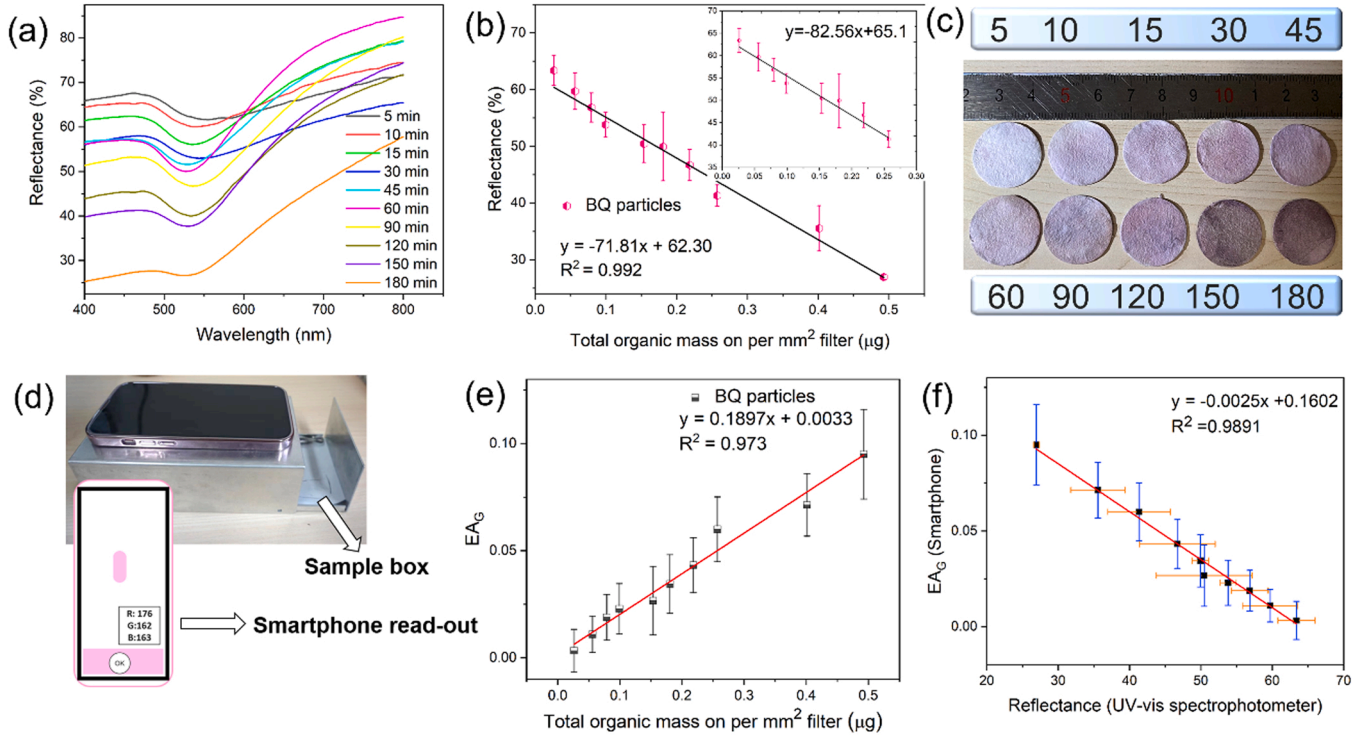


**Fig. 4.** (a) The reflectance spectra of AuNPs@QFs with different concentrations of BQ particles versus wavelength, (b) Plot of the reflectance intensity at 520 nm light wavelength versus concentration of BQ filters, (c) Colors related to standard samples corresponding to (a), (d) Photograph of the smartphone-based device, (e) Plot of $EA_G$ intensity versus total organic mass concentrations of BQ particles loaded on per square millimeter of filters in the range of 0.026–0.49 μg/mm$^2$, (f) Correlation between the analytical signals obtained from the smartphone method and UV–VIS spectrophotometric method for ARC assay.

tested the optical response of a smartphone-based readout device. Fig. 4d depicted the overview of a smartphone-based readout device, where the AuNP-loaded QF was put in the sealed box at a fixed position. Using the digital image processor with the Color Swatch app, the intensities of the RGB components were converted into color pixels which were plotted against total organic mass concentrations of BQ particles loaded on per square millimeter of filters. With the increased BQ concentration, the intensity of red, green and blue decreased. (Fig. S8). The red intensity was higher than that of green and blue, as expected for a pink-violet sample. It should be noted that the color we received was complementary to that which gets absorbed. [6] A pink-violet sample absorbed green light and reflected the red and blue light. The intensity of G, which was a complementary color to the red, decreased more significantly as seen in Fig. S7. Hence, we utilized the G channel for the quantitative investigations. The values of $EA_G = \log (G_b/G_s)$ were selected for the construction of a standard curve in this study. The photography of readout from the smartphone and measured $G_s$ values were shown in Fig. S9 and Table S1. By converting the above color signals into the log ($G_b/G_s$) values, a good linear correlation between log ($G_b/G_s$) and BQ particle concentration was obtained as shown in Fig. 4e ($y = 0.1897x + 0.0033$, $R^2 = 0.973$). The analytical figures of merits about UV–VIS and smartphone-based detection were shown in Table S3. The LOD for the smartphone-based method was determined to be 0.05 μg/mm$^2$. In comparison with the aforementioned spectrophotometric method which was conducted by measuring the UV–VIS reflectance at 520 nm in Fig. 4b, the smartphone assay showed fair linearity. Additionally, there was a good correlation between these two quantification approaches, and the log ($G_b/G_s$) signals and the spectrophotometric reflectance values formed a well-behaved linear relationship with $R^2 = 0.981$ (Fig. 4 f). Good correlation between these two methods validated the reliability of our sensor. These two ARC quantitative approaches also demonstrated outstanding advantages such as simplicity, rapidity, and flexibility. Conventional methods such as the TOC analyzer require additional processes for the extraction of aerosols retained in the filter after sampling for the subsequent analysis of the resultant solution. This makes the analysis more tedious, time-consuming and introduces extra uncertainty. Using smartphones as the detector, our proposed method allowed the ARC concentration to be directly measured on the filters and opened a novel avenue for on-site ARC detection. It is noteworthy that the time of the analysis using the smartphone method was much faster compared to the UV–VIS method and TOC analyzer, usually 20 min for irradiation and less than 30 s for the imaging process since it required no pretreatment and equilibration before testing. Furthermore, the precisions of the developed sensors were further investigated by conducting a 5-times replicate test on the sample of 0.026 μg/mm$^2$ as shown in Table S4. Briefly, the UV-VIS-based method achieved a precision of 4 % while that of the smartphone-based approach was estimated to be 19 %. Due to the complex nature and dynamic behaviour of ARC, our sensor is not as specific as conventional sensors for detecting a single target like protein or nucleic acid. But this proposed methodology directly measures the reducing capability of redox reactants, which means that it is selective and specific for ARC.

### 3.5. Analysis of real-world environmental samples

To test the applicability of the proposed method, 118 real-world aerosol samples collected from three sites of typical environmental settings during December and July were tested and triplicate measurements were conducted for each sample. The measured $G_s$ values were transformed into $EA_G$ and applied in the regression equation to evaluate the ARC concentration in daily samples from the three sites. The details for converting filter concentrations (total organic mass concentrations of BQ particles loaded on per square millimeter filters) into ARC concentrations (ARC mass per unit air volume) were provided in the supporting information S3 and Table S5. For the urban area of Zurich in December, the concentrations of ARC ranged from 1.88 to 9.92 μg•m$^{-3}$, lower than the concentrations of PM10 (3.8–21.6 μg•m$^{-3}$). For Zurich in July, the concentrations of ARC were in the range of 1.34–7.78 μg•m$^{-3}$ while the PM10 concentrations were 6.1–16.6 μg•m$^{-3}$. ARC mass constituted on average 43.3 % of the PM10 mass in December while it was approximately 40.8 % of PM10 in July for Zurich (Fig. 5a and 5b). We noted a similar contribution of ARC to PM10 in Zurich. The average ARC concentration (5.46 μg•m$^{-3)}$ in December was higher than that of ARC (4.49 μg•m$^{-3}$) in July.

As shown in Fig. 5c, we retrieved the ARC concentrations ranging from 3.63 to 9.81 μg•m$^{-3}$ and the PM10 concentrations ranging from 5.8 to 29.4 μg•m$^{-3}$ for Bern in December. Fig. 5d showed that the ARC and the PM10 concentrations changed to 3.87–8.99 μg•m$^{-3}$ and 8.7−18.2 μg•m$^{-3}$ in July. Additionally, ARC mass accounted for on average 42.1 % of PM10 in December, which was lower than the contribution to PM10 (50.3 %) in July. As an urban area, the sampling site in Bern was located in a crossover of trafficked roadside. The relative contribution of different species to the total PM10 mass varied between Zurich and Bern. The relatively high concentrations in Bern compared to Zurich were possibly linked to the high traffic emissions. A relatively large fraction of black carbon, mineral dust and a low fraction of sulphate and ammonium made up ARC and further increased the concentrations of PM10 in Bern [41].

As a high-altitude and low human activity region, Rigi mountain (Fig. 5e and 5f) showed the ARC concentrations within a low-level range from 0.48 to 2.8 μg•m$^{-3}$ in December. It was similar to the range of PM10 (0.5–5 μg•m$^{-3}$). In contrast, ARC concentrations in July were at a relatively high level ranging from 0.27 to 5.7 μg•m$^{-3}$, which accounted for on average 31 % of PM10 mass (2.3–15.5 μg•m$^{-3}$). In comparison to the other two sites (Zurich and Bern), concentrations in Rigi Mountain exhibited low-level ARC and PM10 concentrations.

Of particular interest, we found all of the collected filter samples from the three different sites possessed similar trends with respect to PM10, although the real-world samples were from different environments including the urban area, urban traffic area and rural mountain. The comparison between ARC and PM10 in December and July indicated that ARC concentrations were positive correlation with the concentrations of PM10.

It was previously reported that winter organic aerosols (OA) and summer OA appeared to be associated with the source to some extent. [17,19] Biomass burning organic aerosols (BBOA) have been thought to be a significant source of PM10 in winter time in alpine, suburban and urban areas of Switzerland. [30] BBOA have been reported to exhibit a prominent seasonal variation with a significant increase during winter in Zurich and Bern. Our experimental results acquired by leveraging the proposed LSPR colorimetric technique also confirmed the finding of the seasonality with a maximum in winter and minimum in summer for ARC and PM10 concentrations for the low-elevation Zurich and Bern. Moreover, low temperature could facilitate condensation of volatile compounds and lower vertical mixing, further resulting in high ARC and PM10 concentrations in winter. [43] The enhanced production of secondary organic aerosols (SOA) and biogenic emissions with elevated temperatures dominated in summer, as evidenced by previous studies. [17] However, a reversed pattern of maximum concentrations in summer was observed in Rigi Mountain where anthropogenic sources were not significant. This trend was consistent with the work of Grange et al. and our previous study about Rigi Mountain. [25,52] For the high-altitude, particles are affected by the atmospheric boundary layer, which is the region of occurring exchanges of neat, mass and momentum between the earth's surface and atmosphere. Given that the Rigi site is above 1000 m, the levels of ARC and PM10 are dependent on if the sampling station is within the atmospheric boundary layer or above. [5] In winter, the monitoring sites at Rigi were above the boundary layer and located in the free troposphere decoupled from surface-based emissions. Moreover, the PM10 concentration was inversely related to wind speed. High wind speeds cleaned the atmosphere by dispersing and diluting the aerosol particles and preventing local accumulations, which

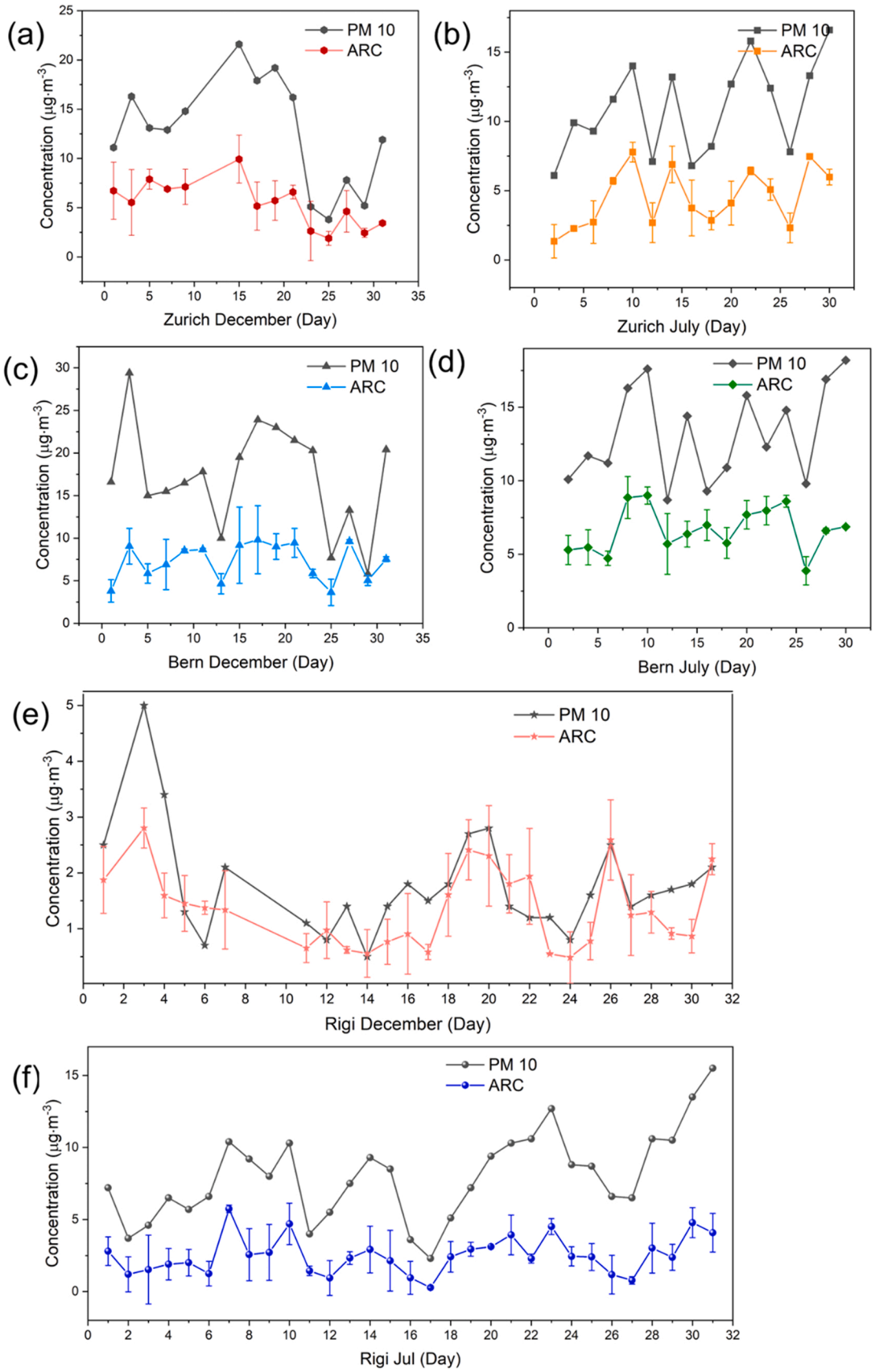


**Fig. 5.** Comparison of daily ARC concentrations at (a) Zurich in December, (b) Zurich in July (c) Bern in December, (d) Bern in July, (e) Rigi Mountain in December and (f) Rigi Mountain in July. The error bars represent the standard deviations for three replicates.

further decreased the levels of ARC and PM10. During summer, these Rigi sites were within the boundary layer, and the relatively well-mixed aerosols contributed to the PM10 levels. Furthermore, strong solar irradiance in summer enhanced the photochemistry of aerosols. Although the general trends of the ARC concentrations in summer and winter obtained were in good agreement with previous measurements, [18,52] the ARC concentrations were consistently lower in Bern and Rigi Mountain than before. This reflected an improvement in air quality within Switzerland possibly due to less biomass burning activities and effective traffic emission control [5].

## 4. Conclusions

In conclusion, a photochemistry-mediated and reduction-based plasmonic colorimetric system was developed for the direct detection of ARC on the filters. This flexible, convenient, and rapid approach combined the technology of in-situ AuNP reduction, plasmonic colorimetry of AuNPs and the reduction ability of ARC. Multifunctional filters were employed as both the filtration substrate with outstanding sampling efficiency, and the reservoir to store reagents for in-situ redox reaction. Upon light irradiation to accelerate the chemical reduction process on the filter, we firstly built a calibration curve based on the reflectance of AuNPs using BQ as the standard model. Subsequently, a portable smartphone-based device was developed as an alternative platform to the UV–VIS spectrophotometer. This approach enabled the real-time and on-site ARC monitoring in the collected airborne particles and possessed a desirable analytical performance (LOD:0.05 $\mu g \bullet mm^{-2}$). Specially, the smartphone-based colorimetric method achieved a good correlation with the spectrophotometric method. Furthermore, the proposed ARC sensing platform was validated by testing real-world environmental samples collected from three different sites in Zurich, Bern and Rigi Mountain. The concentrations of ARC in environmental samples exhibited a positive correlation with that of PM10, and the seasonal trends were in agreement with other previous works. Given the advantages of this proposed sensor system, including the elimination of sample pre-treatment, improved sample-to-detection efficiency, fast on-site ARC quantification, and exemption of using complex and expensive analytical instrumentation, this proposed method can be potentially exploited for fast quantification of ARC to evaluate air quality and potential impact on human health.

## CRediT authorship contribution statement

**Ranxue Yu:** Conceptualization, Methodology, Investigation, Formal analysis, Writing – original draft. **Guangyu Qiu:** Conceptualization, Investigation, Resources, Writing – review & editing, Supervision. **Yi-Bo Zhao:** Investigation, Validation, Data curation, Formal analysis. **Denise Freudemann:** Data curation, Formal analysis. **Beatrice Fisher:** Data curation, Formal analysis. **Xinhou Wang:** Investigation, Writing – review & editing, Funding acquisition. **Jing Wang:** Conceptualization, Resources, Writing – review & editing, Supervision.

## Declaration of Competing Interest

The authors declare that they have no known competing financial interests or personal relationships that could have appeared to influence the work reported in this paper.

## Data Availability

Data will be made available on request.

## Acknowledgments

Ranxue Yu is grateful to China Scholarship Council and Donghua University for the financial support. She also thanks to the National Natural Science Foundation of China (Grant No. 51776034) for the support. Special thanks to my father Bin Yu, for providing suggestions and help with my experiment.

## Appendix A. Supporting information

Supplementary data associated with this article can be found in the online version at doi:10.1016/j.snb.2022.132505.

## References

[1] M. Aeschbacher, D. Vergari, R.P. Schwarzenbach, M. Sander, Electrochemical analysis of proton and electron transfer equilibria of the reducible moieties in humic acids, Environ. Sci. Technol. 45 (19) (2011) 8385–8394.
[2] M. Antiñolo, M.D. Willis, S. Zhou, J.P. Abbatt, Connecting the oxidation of soot to its redox cycling abilities, Nat. Commun. 6 (1) (2015) 1–7.
[3] A. Anwar, A. Minhaz, N.A. Khan, K. Kalantari, A.B.M. Afifi, M.R. Shah, Synthesis of gold nanoparticles stabilized by a pyrazinium thioacetate ligand: A new colorimetric nanosensor for detection of heavy metal Pd (II), Sens. Actuators, B 257 (2018) 875–881.
[4] H. Bai, X. Qian, J. Fan, Y. Shi, Y. Duo, C. Guo, X. Wang, Theoretical model of single fiber efficiency and the effect of microstructure on fibrous filtration performance: a review, Ind. Eng. Chem. Res. 60 (1) (2021) 3–36.
[5] I. Barmpadimos, C. Hueglin, J. Keller, S. Henne, A. Prévôt, Influence of meteorology on PM 10 trends and variability in Switzerland from 1991 to 2008, Atmos. Chem. Phys. 11 (4) (2011) 1813–1835.
[6] L. Byrne, J. Barker, G. Pennarun-Thomas, D. Diamond, S. Edwards, Digital imaging as a detector for generic analytical measurements, TrAC Trends Anal. Chem. 19 (8) (2000) 517–522.
[7] L.F. Capitán-Vallvey, N. López-Ruiz, A. Martínez-Olmos, M.M. Erenas, A.J. Palma, Recent developments in computer vision-based analytical chemistry: a tutorial review, Anal. Chim. Acta 899 (2015) 23–56.
[8] M. Cerrato-Alvarez, S. Frutos-Puerto, C. Miró-Rodríguez, E. Pinilla-Gil, Measurement of tropospheric ozone by digital image analysis of indigotrisulfonate-impregnated passive sampling pads using a smartphone camera, Microchem. J. 154 (2020), 104535.
[9] M. Cerrato-Alvarez, S. Frutos-Puerto, P. Arroyo, C. Miró-Rodríguez, E. Pinilla-Gil, A portable, low-cost, smartphone assisted methodology for on-site measurement of NO2 levels in ambient air by selective chemical reactivity and digital image analysis, Sens. Actuators, B 338 (2021), 129867.
[10] J.G. Charrier, C. Anastasio, On dithiothreitol (DTT) as a measure of oxidative potential for ambient particles: evidence for the importance of soluble transition metals, Atmos. Chem. Phys. 12 (5) (2012) 11317.
[11] J.G. Charrier, C. Anastasio, Rates of hydroxyl radical production from transition metals and quinones in a surrogate lung fluid, Environ. Sci. Technol. 49 (15) (2015) 9317–9325.
[12] X. Chen, P.K. Hopke, W.P.L. Carter, Secondary organic aerosol from ozonolysis of biogenic volatile organic compounds: chamber studies of particle and reactive oxygen species formation, Environ. Sci. Technol. 45 (1) (2011) 276–282.
[13] Y. Chen, M. Takeuchi, T. Nah, L. Xu, M.R. Canagaratna, H. Stark, K. Baumann, F. Canonaco, A.S. Prévôt, L.G. Huey, Chemical characterization of secondary organic aerosol at a rural site in the southeastern US: insights from simultaneous high-resolution time-of-flight aerosol mass spectrometer (HR-ToF-AMS) and FIGAERO chemical ionization mass spectrometer (CIMS) measurements, Atmos. Chem. Phys. 20 (14) (2020) 8421–8440.
[14] M.Y. Chung, R.A. Lazaro, D. Lim, J. Jackson, J. Lyon, D. Rendulic, A.S. Hasson, Aerosol-borne quinones and reactive oxygen species generation by particulate matter extracts, Environ. Sci. Technol. 40 (16) (2006) 4880–4886.
[15] J.B. Conant, L.F. Fieser, Reduction potentials of quinones. ii. the potentials of certain derivatives of benzoquinone, naphthoquinone and anthraquinone, J. Am. Chem. Soc. 46 (8) (1924) 1858–1881.
[16] D.P. Connell, S.E. Winter, V.B. Conrad, M. Kim, K.C. Crist, The steubenville comprehensive air monitoring program (SCAMP): concentrations and solubilities of PM2. 5 trace elements and their implications for source apportionment and health research, J. Air Waste Manag. Assoc. 56 (12) (2006) 1750–1766.
[17] K.R. Daellenbach, G. Stefenelli, C. Bozzetti, A. Vlachou, P. Fermo, R. Gonzalez, A. Piazzalunga, C. Colombi, F. Canonaco, C. Hueglin, Long-term chemical analysis and organic aerosol source apportionment at nine sites in central Europe: source identification and uncertainty assessment, Atmos. Chem. Phys. 17 (21) (2017) 13265–13282.
[18] K.R. Daellenbach, G. Uzu, J. Jiang, L.-E. Cassagnes, Z. Leni, A. Vlachou, G. Stefenelli, F. Canonaco, S. Weber, A. Segers, Sources of particulate-matter air pollution and its oxidative potential in Europe, Nature 587 (7834) (2020) 414–419.
[19] K.R. Daellenbach, C. Bozzetti, A. Křepelová, F. Canonaco, R. Wolf, P. Zotter, P. Fermo, M. Crippa, J.G. Slowik, Y. Sosedova, Y. Zhang, R.J. Huang, L. Poulain, S. Szidat, U. Baltensperger, I. El Haddad, A.S.H. Prévôt, Characterization and source apportionment of organic aerosol using offline aerosol mass spectrometry, Atmos. Meas. Tech. 9 (1) (2016) 23–39.
[20] R.J. Delfino, C. Sioutas, S. Malik, Potential role of ultrafine particles in associations between airborne particle mass and cardiovascular health, Environ. Health Perspect. 113 (8) (2005) 934–946.

[21] J.M. Delgado-Saborit, M.S. Alam, K.J.G. Pollitt, C. Stark, R.M. Harrison, Analysis of atmospheric concentrations of quinones and polycyclic aromatic hydrocarbons in vapour and particulate phases, Atmos. Environ. 77 (2013) 974–982.
[22] S. Du, Y. Luo, Z. Liao, W. Zhang, X. Li, T. Liang, F. Zuo, K. Ding, New insights into the formation mechanism of gold nanoparticles using dopamine as a reducing agent, J. Colloid Interface Sci. 523 (2018) 27–34.
[23] H. ElBishlawi, P.R. Jaffe, Characterization of dissolved organic matter from a restored urban marsh and its role in the mobilization of trace metals, Chemosphere 127 (2015) 144–151.
[24] G. Garcia, A.G. Allen, A.A. Cardoso, A new and simple visual technique based on indigo dye for determination of ozone in ambient air, Water Air Soil Pollut. 225 (2) (2014) 1836.
[25] S.K. Grange, D.C. Carslaw, A.C. Lewis, E. Boleti, C. Hueglin, , Random forest meteorological normalisation models for Swiss PM 10 trend analysis, Atmos. Chem. Phys. 18 (9) (2018) 6223–6239.
[26] L. Guo, S. Chen, Y.-L. Yu, J.-H. Wang, A. Smartphone, Optical device for point-of-care testing of glucose and cholesterol using Ag NPs/UiO-66-NH2-based ratiometric fluorescent probe, Anal. Chem. 93 (48) (2021) 16240–16247.
[27] R.J. Hopkins, A.V. Tivanski, B.D. Marten, M.K. Gilles, Chemical bonding and structure of black carbon reference materials and individual carbonaceous atmospheric aerosols, J. Aerosol Sci. 38 (6) (2007) 573–591.
[28] Y. Kumagai, S. Koide, K. Taguchi, A. Endo, Y. Nakai, T. Yoshikawa, N. Shimojo, Oxidation of proximal protein sulfhydryls by phenanthraquinone, a component of diesel exhaust particles, Chem. Res. Toxicol. 15 (4) (2002) 483–489.
[29] P.S. Lakey, T. Berkemeier, H. Tong, A.M. Arangio, K. Lucas, U. Pöschl, M. Shiraiwa, Chemical exposure-response relationship between air pollutants and reactive oxygen species in the human respiratory tract, Sci. Rep. 6 (1) (2016) 1–6.
[30] V.A. Lanz, M.R. Alfarra, U. Baltensperger, B. Buchmann, C. Hueglin, S. Szidat, M. N. Wehrli, L. Wacker, S. Weimer, A. Caseiro, H. Puxbaum, A.S.H. Prevot, Source attribution of submicron organic aerosols during wintertime inversions by advanced factor analysis of aerosol mass spectra, Environ. Sci. Technol. 42 (1) (2008) 214–220.
[31] H. Li, X. Wang, X. Li, H.-Z. Yu, Quantitative pH determination based on the dominant wavelength analysis of commercial test strips, Anal. Chem. 93 (46) (2021) 15452–15458.
[32] P. Lin, J.Z. Yu, Generation of reactive oxygen species mediated by humic-like substances in atmospheric aerosols, Environ. Sci. Technol. 45 (24) (2011) 10362–10368.
[33] Z. Liu, P. Xie, J. Ma, Aqueous photoproduction of Au nanoparticles by natural organic matter: effect of NaBH4 reduction, Environ. Sci.: Nano 3 (4) (2016) 707–714.
[34] Y. Lyu, H. Guo, T. Cheng, X. Li, Particle size distributions of oxidative potential of lung-deposited particles: assessing contributions from quinones and water-soluble metals, Environ. Sci. Technol. 52 (11) (2018) 6592–6600.
[35] M.L. Machesky, W.O. Andrade, A.W. Rose, Interactions of gold (III) chloride and elemental gold with peat-derived humic substances, Chem. Geol. 102 (1–4) (1992) 53–71.
[36] R.D. McWhinney, K. Badali, J. Liggio, S.-M. Li, J.P. Abbatt, Filterable redox cycling activity: a comparison between diesel exhaust particles and secondary organic aerosol constituents, Environ. Sci. Technol. 47 (7) (2013) 3362–3369.
[37] A. Mechler, A.A. Torriero, A. Nafady, C.-Y. Lee, A.M. Bond, A.P. O'Mullane, S. K. Bhargava, The formation of gold nanoparticles using hydroquinone as a reducing agent through a localized pH change upon addition of NaOH to a solution of HAuCl4, Colloids Surf., A 370 (1–3) (2010) 35–41.
[38] L. Ntziachristos, J.R. Froines, A.K. Cho, C. Sioutas, Relationship between redox activity and chemical speciation of size-fractionated particulate matter, Part. Fibre Toxicol. 4 (1) (2007) 1–12.
[39] Y. Ohara, K. Akazawa, K. Shibata, T. Hirota, Y. Kodama, T. Amemiya, J. Wang, T. Yamaguchi, Seed-mediated gold nanoparticle synthesis via photochemical reaction of benzoquinone, Colloids Surf., A 586 (2020), 124209.
[40] M. Paglione, A. Kiendler-Scharr, A.A. Mensah, E. Finessi, L. Giulianelli, S. Sandrini, M.C. Facchini, S. Fuzzi, P. Schlag, A. Piazzalunga, Identification of humic-like substances (HULIS) in oxygenated organic aerosols using NMR and AMS factor analyses and liquid chromatographic techniques, Atmos. Chem. Phys. 14 (1) (2014) 25–45.
[41] J.-P. Putaud, F. Raes, R. Van Dingenen, E. Brüggemann, M.-C. Facchini, S. Decesari, S. Fuzzi, R. Gehrig, C. Hüglin, P. Laj, A European aerosol phenomenology—2: chemical characteristics of particulate matter at kerbside, urban, rural and background sites in Europe, Atmos. Environ. 38 (16) (2004) 2579–2595.
[42] P. Sachinidou, Y.K. Bahk, M. Tang, N. Zhang, S.S.C. Chen, D.Y.H. Pui, B.A. Lima, G. Bosco, P. Tronville, T. Mosimann, M. Eriksson, J. Wang, Inter-laboratory validation of the method to determine the filtration efficiency for airborne particles in the 3–500 nm range and results sensitivity analysis, Aerosol Air Qual. Res 17 (11) (2017) 2669–2680.
[43] V. Samburova, T. Didenko, E. Kunenkov, C. Emmenegger, R. Zenobi, M. Kalberer, Functional group analysis of high-molecular weight compounds in the water-soluble fraction of organic aerosols, Atmos. Environ. 41 (22) (2007) 4703–4710.
[44] C. Shan, H. Yang, D. Han, Q. Zhang, A. Ivaska, L. Niu, Graphene/AuNPs/chitosan nanocomposites film for glucose biosensing, Biosens. Bioelectron. 25 (5) (2010) 1070–1074.
[45] S.S. Shankar, A. Rai, B. Ankamwar, A. Singh, A. Ahmad, M. Sastry, Biological synthesis of triangular gold nanoprisms, Nat. Mater. 3 (7) (2004) 482–488.
[46] S.E. Skrabalak, J. Chen, Y. Sun, X. Lu, L. Au, C.M. Cobley, Y. Xia, Gold nanocages: synthesis, properties, and applications, Acc. Chem. Res. 41 (12) (2008) 1587–1595.
[47] R. Srisukjaroen, K. Wechakorn, S. Teepoo, A smartphone based-paper test strip chemosensor coupled with gold nanoparticles for the Pb2+ detection in highly contaminated meat samples, Microchem. J. 179 (2022), 107438.
[48] M. Turner, V.B. Golovko, O.P.H. Vaughan, P. Abdulkin, A. Berenguer-Murcia, M. S. Tikhov, B.F.G. Johnson, R.M. Lambert, Selective oxidation with dioxygen by gold nanoparticle catalysts derived from 55-atom clusters, Nature 454 (7207) (2008) 981–983.
[49] V. Verma, Y. Wang, R. El-Afifi, T. Fang, J. Rowland, A.G. Russell, R.J. Weber, Fractionating ambient humic-like substances (HULIS) for their reactive oxygen species activity–Assessing the importance of quinones and atmospheric aging, Atmos. Environ. 120 (2015) 351–359.
[50] S. Viswanathan, D. Rothamer, A. Zelenyuk, M. Stewart, D. Bell, Experimental investigation of the effect of inlet particle properties on the capture efficiency in an exhaust particulate filter, J. Aerosol Sci. 113 (2017) 250–264.
[51] Y. Yin, S. Yu, J. Liu, G. Jiang, Thermal and photoinduced reduction of ionic Au (III) to elemental Au nanoparticles by dissolved organic matter in water: Possible source of naturally occurring Au nanoparticles, Environ. Sci. Technol. 48 (5) (2014) 2671–2679.
[52] R. Yu, F. Pan, C. Schreine, X. Wang, D.M. Bell, G. Qiu, J. Wang, Quantitative determination of airborne redox-active compounds based on heating-induced reduction of gold nanoparticles, Anal. Chem. 93 (44) (2021) 14859–14868.
[53] X. Yuan, A.N. Pham, C.J. Miller, T.D. Waite, Copper-catalyzed hydroquinone oxidation and associated redox cycling of copper under conditions typical of natural saline waters, Environ. Sci. Technol. 47 (15) (2013) 8355–8364.
[54] M. Zhu, J. Lu, Y. Hu, Y. Liu, S. Hu, C. Zhu, Photochemical reactions between 1, 4-benzoquinone and O2•−, Environ. Sci. Pollut. Res. 27 (25) (2020) 31289–31299.

**Ranxue Yu** is currently a Ph.D. candidate at College of Textiles, Donghua University, China. Her research focuses on the detection of airborne redox-active compounds based on gold nanoparticles, comparison of oxidative potential of aerosols from different origins and development of metal-coated nanofibers.

**Guangyu Qiu** is a postdoctoral Researcher at ETH Zurich. He obtained his Ph.D. from City University of Hong Kong. His research area includes applied optics and plasmonic, functional materials in nano-optics, chemical, biochemical and environmental sensing applications.

**Yi-Bo Zhao** is currently pursuing his Ph.D. degree under the direction of Prof. Jing Wang at the Institute of Environmental Engineering, ETH Zürich. His research interests include aerosol sampling, aerosol trace metal determination, electrochemical sensors, and development of integrated aerodynamic/electrochemical sensing system.

**Denise Freudemann** is a technician at Eawag, Swiss Federal Institute of Aquatic Science and Technology. She is responsible for water physicochemical measurements.

**Beatrice Fisher** is a technician at Empa. She is responsible for the measurements of various materials, including mechanical test, FITR.

**Xinhou Wang** is a professor at College of Textiles, Donghua University. His research interests including the preparation of functional melt-blown nonwovens and spinning mechanism, stab-proof clothes and stab mechanism and compact spinning.

**Jing Wang** is an associate professor at the Institute of Environmental Engineering in the Department of Civil, Environmental and Geomatics Engineering, ETH Zürich. He received his Ph.D. degree in Aerospace Engineering at the University of Minnesota in 2005. He worked as a postdoctoral associate in the Particle Technology Laboratory, Mechanical Engineering at the University of Minnesota. His research interests include air pollution control, nanoparticle transport and emission reduction, instrumentation for airborne nanoparticle measurement, air and water filtration, and mechanics of multiphase flow.